Supplementary Information

Trident cold atmospheric plasma blocks three cancer survival pathways to overcome therapy resistance

Bo Guo[a,b,1], Anthony D. Pomicter[c,1], Francis Li[a], Sudhir Bhatt[a], Chen Chen,[a,d], Wen Li[b], Miao Qi[d], Chen Huang[b], Michael W. Deininger[c,e], Michael G. Kong[a,f,2,3] and Hai-Lan Chen[a,2,3]

[a]Frank Reidy Center for Bioelectrics, Old Dominion University, Norfolk, VA, USA
[b]Department of Cell Biology and Genetics, School of Basic Medical Sciences, Xi'an Jiaotong University, Health Science Center, Xi'an, Shaanxi, P R China
[c]Huntsman Cancer Institute, University of Utah, Salt Lake City, UT, USA
[d]State Key Laboratory of Electrical Insulation and Power Equipment, Center for Plasma Biomedicine, Xi'an Jiaotong University, Xi'an, Shaanxi, P R China
[e]Division of Hematology and Hematologic Malignancies, University of Utah, Salt Lake City, UT, USA
[f]Department of Electrical and Computer Engineering, Old Dominion University, Norfolk, VA, USA
[1]These authors contributed equally to this work.
[2]These authors contributed equally to this work.

[3]Correspondence to Michael. G. Kong and Hai-Lan Chen
E-mail: mkong@odu.edu, h1chen@odu.edu

This PDF file includes:

Materials and Methods

Measurement of extracellular ROS in cell-free medium. Long-lived reactive oxygen species (ROS) produced by trident cold atmospheric plasma (Tri-CAP) in cell-free RPMI-1640 medium (Gibco Life Technologies, Thermo Fisher Scientific, Waltham. MA, USA) were measured using a microplate reader (FLUOStar, BMG Labtech, Cary, NC, USA) with the Amplex Red Hydrogen Peroxide/Peroxidase Assay Kit (Thermo Fisher Scientific) for H_2O_2 and the Griess Reagent Nitrate/Nitrite Colorimetric Assay Kit (Cayman Chemical Co, Ann Arbor, MI, USA) for nitrite (NO_2^-) and nitride (NO_3^-). Short-lived ROS were measured with an electron spin resonance (ESR) spectrometer (EMX+, Bruker, Germany) and the following spin traps: 5,5-dimethyl-1-pyrroline N-oxide (DMPO; Dojindo Laboratories, Japan) for $^{\bullet}OH$, N-(dithiocarboxy)sarcosine (DTCS) and N-methyl-d-glucamine dithiocarbamate (MGD; Dojindo Laboratories, Japan) for $^{\bullet}NO$, 2,2,6,6-tetramethylpiperidine (TEMP; Sigma-Aldrich, St. Louis, MO, USA) for $^1O_2$, and 1-hydroxy-2,2,6,6-tetramethyl-4-oxo-piperidine (TEMPONE-H; Enzo Biochem, Farmingdale, NY, USA) for $O_2^{\bullet-}$ and $ONOO^-$. Spin trap concentrations were chosen based on dosing experiments. For 60-s Tri-CAP treatment, 5-mM TEMPONE-H was found to be adequate for trapping $ONOO^-$ and $O_2^{\bullet-}$. For TEMP and DMPO, we chose 30 mM and 50 mM, respectively. Spin traps were added to RPMI-1640 medium before and after Tri-CAP treatment for measurement of ROS produced during the treatment and residual ROS post-treatment, respectively. NAC (N-Acetyl-L-cysteine; Sigma-Aldrich) was used to scavenge ROS.

Murine and human cell lines. Mouse Ba/F3 cell lines with the BCR-ABL1^{p210} and BCR-ABL1^{T315I} mutations are sensitive and resistant to imatinib, respectively (1). These were maintained in RPMI-1640 medium, supplemented with 10% fetal bovine serum (FBS; Atlanta Biologicals, R&D Systems, Minneapolis, MN, USA), 4-mM L-glutamine (Gibco Life Technologies), and a mixture of streptomycin (100 μg/mL) and penicillin (100 U/mL) (Gibco Life Technologies) at 37°C in 5% CO_2. The culture medium for Ba/F3 parental cells was the same as above but also contained 10% of WEHI cell culture supernatant as a source of mouse interleukin (IL)-3. Parental Ba/F3 cells are insensitive to imatinib.

Human chronic myeloid leukemia (CML) imatinib-sensitive AR230^S cells (CRL-3345; American Type Culture Collection [ATCC], Manassas, VA, USA) and human breast cancer BT-474 Clone 5 cells (CRL-3247; ATCC) were maintained in RPMI-1640 medium, supplemented with 10% FBS (Atlanta Biologicals) and a mixture of streptomycin (100 μg/ml) and penicillin (100 U/mL) at 37°C in 5% CO_2. Imatinib-resistant human CML AR230^R cells were derived by long-term culture in the presence of low-dose imatinib, followed by incremental increases in concentration (0.1–1.0 μM) and maintenance of a single clone in continual 1.0-μM imatinib (Sigma-Aldrich), with isogenic AR230S cells used as controls. Human

malignant melanoma A-375 cells (CRL-1619; ATCC) are cultured in Dulbecco's Modified Eagle's Medium (DMEM; ATCC), with 10% FBS (Atlanta Biologicals) and a mixture of streptomycin (100 μg/ml) and penicillin (100 U/mL) (Gibco Life Technologies) at 37°C in 5% CO_2.

Intracellular ROS measurement. Approximately 1.5×10^5 cells/mL in 2-mL culture media were incubated with fluorescent dye at 37°C. Incubation times for optimal dye signals were 15–45 min, depending on ROS. Cells were then pelleted by centrifugation at 200 x g for 5 min, washed with phosphate-buffered saline (PBS) to remove excess dyes, and re-suspended in fresh media. Suspensions of untreated and treated cells were analyzed by flow cytometry (NovoCyte, ACEA biosciences, San Diego CA, USA). The following fluorescent dyes were used in these experiments: dihydroethidium at 1 μM for $O_2^{\bullet-}$, DAF-FM diacetate at 10 μM for $^{\bullet}NO$, 3'-(p-hydroxyphenyl) fluorescein at 5 μM for $ONOO^-$, and CM-H_2DCFDA at 20 μM for general ROS (all from Thermo Fisher Scientific).

Measurement of total antioxidant capacity and glutathione to oxidized glutathione ratio. Ba/F3 cell lines were seeded into 12-well plates at a density of 1.5×10^5/mL and treated with Tri-CAP or control. After 24 and 72 h, cells were distributed into 96-well plates, and cellular antioxidant systems were measured using the Total Antioxidant Capacity Assay (Abcam, Cambridge, UK) and the GSH/GSSG-Glo Assay (Promega, Madison, WI, USA).

RNA extraction, cDNA synthesis, and quantitative reverse transcription PCR (qRT-PCR). Cells were treated with Tri-CAP or control, and at 6, 12, 24, and 48 h post-treatment, cells were harvested for total RNA extraction using the AllPrep DNA/RNA/Protein Mini Kit (QIAGEN, Hilden, Germany). Quantity and quality of all RNA samples was assessed by measuring optical density at 260 and 280 nm. For cDNA synthesis, total RNA (1 μg) was reverse transcribed using the High-Capacity cDNA Reverse Transcription Kit (Applied Biosystems, Foster City, CA, USA), according to the manufacturer instructions. To specifically quantify expression of target genes, cDNA dilutions (1:10) were mixed with SsoAdvanced™ Universal SYBR® Green Supermix (Bio-Rad, Hercules, CA. USA) and gene-specific PCR amplification reactions were conducted in a T100™ Thermal Cycler (Bio-Rad). Relative gene expression was quantified using the $2^{-\Delta\Delta ct}$ methods, with *GAPDH* as the reference gene. The following primers were used: *Ldha*-Forward: 5'- GGATGAGCTTGCCCTTGTTGA-3', *Ldha*-Reverse: 5'-GACCAGCTTGGAGTTCGCAGTTA-3'; *Pdk1*-Forward: 5'-GACTGTGAAGATGAGTGACCG-3', *Pdk1*-Reverse: 5'-CAATCCGTAACCAAACCCAG-3'; *Pdk3* Forward: 5'-TCCTGGACTTCGGAAGGGATA-3', *Pdk3* Reverse: 5'-GAAGGGCGGTTCAACAAGTTA-3'; *Hk1*-Forward: 5'-GAGTCTGAGGTCTACGACACC-3', *Hk1*-Reverse: 5'-CCCACGGGTAATTTCTTGTCC-

3'; *Hk2*-Forward: 5'-ATGATCGCCTGCTTATTCACG-3', *Hk2*-Reverse: 5'-CGCCTAGAAATCTCCAGAAGGG-3'; *Glut1*-Forward: 5'-GGGCATGTGCTTCCAGTATGT-3', *Glut1*-Reverse: 5'-ACGAGGAGCACCGTGAAGAT-3'; *GAPDH*-Forward: 5'-GGCATTGCTCTCAATGACAA-3', *GAPDH*-Reverse: 5'-TGTGAGGGAGATGCTCAGTG-3'.

Western blot analysis. Total protein from Tri-CAP- and control-treated cells was extracted in cell lysis buffer with a cocktail of phosphatase inhibitors and protease inhibitors (Cell Signaling Technology, Danvers, MA, USA) and separated by 10% SDS polyacrylamide gel electrophoresis (SDS-PAGE; Bio-Rad). Separated proteins were electrophoretically transferred to polyvinylidene difluoride (PVDF) membranes (MilliporeSigma, Burlington, MA, USA). After blocking with 5% nonfat milk, membranes were incubated overnight at 4°C with primary antibodies from the Glycolysis Antibody Sampler Kit, mTOR Pathway Antibody Sampler Kit, and Phospho-Akt Pathway Antibody Sampler Kit (all from Cell Signaling Technology) and anti-β-actin antibody (Li-Cor Biosciences, Lincoln, NE, USA). Membranes were washed with TBST buffer for three times (10 mins each time) and then incubated with anti-rabbit IgG, horseradish peroxidase (HRP)-linked secondary antibody (Cell Signaling Technology) for 2 h at room temperature. Blots were scanned, and band densities were measured with an enhanced chemiluminescence detection system (Bio-Rad). Antibodies are listed in Table S4.

Dose-dependent effect of H_2O_2 on apoptosis and HIF-1α expression. BCR-ABL1^{T315I} cells were seeded in 12-well plates at a density of 7.5×10^4/mL in triplicate, and then incubated with H_2O_2 (Beyotime, Beijing, China) at a final concentration of 0, 5, 10, 25, 50, 100 or 200 μM for 24 h. For apoptosis assay, cells were stained with propidium iodide (PI) and Annexin V-FITC according to the manufacturer's instruction (Beyotime), and analyzed by flow cytometry (BD Accuri C6, Frankin Lakes, NJ, USA). For HIF-1α expression detection, protein from H_2O_2 treated cells was separated, transferred to PVDF membranes and incubated with primary antibody (anti-HIF-1α, Cell Signaling Technology) by western blot analysis as described previously.

Measurement of lactate production. Lactate was measured using Lactate Assay Kit (Sigma-Aldrich) according to the manufacturer instructions. Lactate standard curve samples were prepared in duplicate, at final concentrations of 0, 25, 50, 100, 200, 400, 600, and 1,000 μM. Samples were incubated for 20 min at room temperature and then measured with a microplate reader using an excitation wavelength of 530–540 nm and reading an emission wavelength of 585–595 nm.

Cell Proliferation, apoptosis, and colony formation assays. Ba/F3 cells and derivative lines were seeded into 12-well plates at a density of 1.5 x 10^5/mL and treated with Tri-CAP or control. After 24, 48 and 72 h, cells were distributed in 96-well plates and the 3-(4,5-dimethylthiazol-2-yl)-2,5-diphenyl tetrazolium bromide (MTT) assay was performed following the instruction of the Vybrant® MTT Cell Proliferation Assay Kit (Invitrogen, Thermo Fisher Scientific). Primary cells from healthy individuals and CML patients were distributed in 12-well plates at a density of 5 × 10^4/mL and then treated with Tri-CAP or control. Viable cells were counted by trypan-blue dye exclusion staining under a microscope in triplicate of each well at different times post treatment (1).

Apoptosis was analyzed with the FITC Annexin V/Dead Cell Apoptosis Kit (Invitrogen, Thermo Fisher Scientific). Cells were seeded in 12-well plates at a density of 1.5 × 10^5/mL in triplicate, treated with Tri-CAP for 24 h, and analyzed by flow cytometry (NOVOcyte, Agilent, Technologies, Santa Clara, CA, USA). For colony formation assays, control and Tri-CAP-treated primary $CD34^+$ cells were cultured, and 1 x 10^3 viable cells were seeded into 3-cm^2 dishes with methylcellulose (Stem Cell Technologies, Vancouver, Canada) at a medium:methylcellulose ratio of 1:9, in the presence of rhIL-3 (20 ng/mL), rhIL-6 (20 ng/mL), rhFlt-3 ligand (100 ng/mL), and rhSCF (100 ng/mL) and grown for 7–14 days.

Apoptosis and necroptosis assays to test different cell deaths. Caspase inhibitor (Z-VAD-FMK, HY-16658B) and necroptosis inhibitor (Necrostatin-1, HY-15760) were obtained from MedChemExpress (Monmouth Junction, NJ, USA). Either inhibitor was used to treat BCR-$ABL1^{T315I}$ Cells in a dosing experiment to select 20 μM for Z-VAD-FMK and 2 μM for Necrostatin-1. Ba/F3 BCR-$ABL1^{T315I}$ cells were seeded into 12-well plates at a density of 10^6/mL and treated with Tri-CAP for 60 s and then incubated for 24 h without or with one inhibitor (either 20-μM Z-VAD-FMK or 2-μM Necrostatin-1). Subsequently, necrotic or apoptotic cell population was determined with the Annexin V-FITC/PI assay kit (Invitrogen).

Assessment of ferroptosis. Ba/F3 BCR-$ABL1^{T315I}$ cells were seeded into 12-well plates at a density of 1 × 10^6/mL and treated with 60-s Tri-CAP, 2-μM ferroptosis inducer (Erastin, HY-15763, MedChemExpress), or 1-μM ferroptosis inhibitor (Ferrostatin-1, HY-100579, MedChemExpress). After 24 h, the intracellular iron concentration was assessed using an iron colorimetric assay kit according to the manufacturer's instructions (Applygen, Beijing, China). For detection of NCOA4, Keap-1 and GPX4 expression, protein from treated cells (without or with ferrostatin-1) was separated, transferred to PVDF membranes and incubated with relevant antibody (Table S4) by western blot analysis as described previously.

Mouse tumor model of CML. BALB/c nude mice (male, 3–4 weeks old, approximately 15–16 g) were purchased from SLAC Laboratory (Shanghai, China) and bred in a pathogen-free environment, in

accordance with the Xi'an Jiaotong University guidelines for use of laboratory animals. All animal experiments were approved by the Institutional Animal Care and Use Committee of Xi'an Jiaotong University. Mice were randomly allocated to control and experimental groups (n = 5/group). Using a well-established engraft tumor model (2), Ba/F3 cells with native BCR-ABL1^{P210} or BCR-ABL1^{T315I} were untreated or treated with Tri-CAP and then pooled in equal number of 5 × 10^6 cells/ml suspension before their subcutaneous injection in 100-μl PBS into the flanks of nude mice (Left flank: Tri-CAP; Right flank: untreated). Tumor size was examined with calipers every three days, and tumor volume (mm^3) was calculated as volume (V) = length (L) x width $(W)^2$ x 0.5. Tumor size data were analyzed using paired *t*-tests with GraphPad PRISM software (San Diego, CA, USA). On the last day of the experiment, bioluminescence images of mice were obtained with an IVIS Spectrum (Xenogen, Alameda, CA, USA).

Mouse survival model of CML. BALB/c nude mice (male, 3–4 weeks, approximately 15–16 g) were purchased from SLAC Laboratory (Shanghai, China) and bred in a pathogen-free environment, as described above. These were randomly divided into to the control and experiment groups (n = 5/group). Using a well-established CML survival model (2), Ba/F3 BCR-ABL1^{T315I} or Ba/F3 BCR-ABL1^{P210} cells either untreated (the control group) or treated with Tri-CAP were prepared in equal number (5 × 10^6 cells/ml suspension in PBS) before their injection in 100-μl PBS into the tail vein of nude mice. The weight of each mouse was measured, and their general conditions were monitored every three days post-injection. On necropsy, mice showed complications associated with leukemia (e.g., enlarged liver and/or spleen, tiny red spots in skin, easy bleeding). Survival data were analyzed using the Kaplan Meier method, and statistical significance was evaluated with a log rank test (GraphPad PRISM) comparing survival time of the Tri-CAP group with the control group.

Mouse model of established tumors with Tri-CAP treatment. Male BALB/c mice were obtained from the Experimental Animal Center of Xi'an Jiaotong University and bred under specific pathogen-free conditions. Luciferase-tagged BCR-ABL1^{T315I} cells (1.5 x 10^6 in 100-μl PBS) were injected subcutaneously into the rear dorsum of each mouse and allowed to form tumor for six days when a subcutaneous nodule was clearly seen. Then the mice were randomly divided into two groups of 5 mice each: the control (Ctrl) group without any treatment and the Tri-CAP group with one 120-s treatment every three days with the first treatment on day 6. Tumor volume was measured with a vernier caliper using volume (V) = length (L) x width $(W)^2$ x 0.5 and once every three days. For tumor size comparison on day 18, unpaired t-test with GraphPad was used. For bioluminescence imaging, we used D-Luciferin (HY-12591B, MedChemExpress) as a substrate for luciferase and each animal was injected intraperitoneally with D-Luciferin at a dose of 150 mg per kg in 100 μl PBS. After 5 min, bioluminescent images were acquired on day 9, 18 and 21,

respectively, with an IVIS Spectrum Imaging system (Xenogen, Alameda, CA, USA). The survival time of each mouse was recorded and analyzed using the Kaplan Meier method, and statistical significance was evaluated with a log rank test (GraphPad).

Mouse model of established tumors with PAS treatment. PAS was freshly prepared in saline pretreated by Tri-CAP for 120 s, and saline was used as the vehicle control. Similar to the study of Tri-CAP treatment of established tumor, male BALB/c mice were obtained, bred and injected with luciferase-tagged BCR-ABL1^{T315I} cells. Then, mice were randomly divided into two groups of 5 animal each: the saline group and the PAS group with the pericarcinomatous tissue of each mouse injected with 200-μl saline or 200-μl PAS once every three days from day 6. Then the tumor size, bioluminescent images and survival data were obtained and analyzed in the same way as described above for the study of Tri-CAP treatment of established tumor. All animal studies were approved by the laboratory animal care committee of Xi'an Jiaotong University and performed according to the committee's guidelines for the use of laboratory animals.

Statistical analysis. Individual data points are plotted in most graphs, with the exception of *SI Appendix* Figs. S3, S6, S9, S10, S13-S15, S21D and S22D, which are plotted as mean ± standard deviation (SD). All results were obtained from at least three independent experiments. Data displayed a normal distribution and were analyzed with the unpaired Student's *t*-test (GraphPad Prism v.6.0) unless otherwise stated. Statistical significance was determined with the Holm-Sidak method, unless otherwise stated. $P < 0.05$ was considered statistically significant.

Table S1. Cancer cell viability and H_2O_2 after dielectric barrier discharge (DBD) treatment

Gas	Cell line	Treatment Time	H_2O_2 (μM)	Cell Viability	Ref.
Air	CT26, Colon	10 s	61	43%	3
Air	CT26, Colon	11 s	67	41%	3
Air	U87MG, Glioblastoma	60 s	10	61%	4, 5
Air	U87MG, Glioblastoma	120 s	18	26%	4, 5
Air	LN18, Glioblastoma	60 s	10	48%	4, 5
Air	LN18, Glioblastoma	120 s	18	34%	4, 5
Air	LN229, Glioblastoma	60 s	10	54%	4, 5
Air	LN229, Glioblastoma	120 s	18	42%	4, 5
Air	H460, Lung	1 min	59	79%	6
Air	H460, Lung	5 min	143	38%	6
He	Bel 7402, Cervical	60 s	6.5	60%	7
He	A375, Melanoma	1 min	1248	71%	8
He	A375, Melanoma	3 min	3863	2%	8
Air	SW620, Colorectal	9 min	98	53%	9
Air	SW620, Colorectal	9 min	151	22%	9
Air	Jurkat, Leukemia	10 s	74	70%	10
Air	THP-1, Leukemia	10 s	74	100%	10

Table S2. Cancer cell viability and H_2O_2 after treatment with CAP jets

Gas	Cell line	Treatment Time	H_2O_2 (μM)	Cell Viability	Ref.
Air	Hela, Cervical	210 s	79	14%	11
N_2+H_2O	G361, Melanocytes	3 min	32	63%	12
N_2+H_2O	G361, Melanocytes	5 min	45	26%	12
Ar	LP-1, Myeloma	20 s	9	70%	13
N_2+H_2O	SK-BR3, Breast	5 min	44	17%	14
He	HCT116, Colorectal	2 min	713	45%	15
He	U87MG, Glioblastoma	120 s	14	34%	16
He	B16-BL6, Melanoma	90 s	72	18%	17
He	U87, Glioblastoma	60 s	12	19%	18
He	MDA-MB-231, Breast	60 s	12	6%	18
He	U87, Glioblastoma	60 s	8	96%	18
He	MDA-MB-231, Breast	60 s	8	86%	18
Ar	CT26, Colon	120 s	116	41%	3
He	B16F10, Melanoma	40 s	34	30%	19
Air	4T1, Breast	40 s	1094	17%	20
Air	MCF7, Breast	60 s	287	79%	21
Air	MCF7, Breast	120 s	1149	9%	21
Air	HT-1376, Bladder	60 s	287	21%	21
Air	HT-1376, Bladder	120 s	1149	8%	21
Air	H1299, Lung	60 s	287	47%	21
Air	H1299, Lung	120 s	1149	4%	21
Air	WiDr, Colon	60 s	287	107%	21
Air	WiDr, Colon	120 s	1149	65%	21
Air	HCC1806, Breast	60 s	1368	104%	21
Air	HCC1806, Breast	120 s	2391	38%	21
Air	LnCAP, Prostate	60 s	1368	10%	21

Air	LnCAP, Prostate	120 s	2391	7%	21
Air	ECC-1, Endometrial	60 s	1368	28%	21
Air	ECC-1, Endometrial	120 s	2391	9%	21
Air	TFK-1, Extrahepatic bile duct	60 s	1908	15%	21
Air	TFK-1, Extrahepatic bile duct	120 s	3655	4%	21
Air	PC3, Prostate	60 s	828	9%	21
Air	PC3, Prostate	120 s	1126	3%	21
Air	OE19, Esophageal	60 s	368	56%	21
Air	OE19, Esophageal	120 s	690	17%	21
Air	A375, Melanoma	60 s	368	53%	21
Air	A375, Melanoma	120 s	690	9%	21
Air	MNNG-HOS, Osteosarcoma	60 s	368	31%	21
Air	MNNG-HOS, Osteosarcoma	120 s	690	14%	21

Table S3. Cancer cell viability and H_2O_2 after plasma-activated solution (PAS) treatment

Gas	Cell line	Treatment Time	H_2O_2 (μM)	Cell Viability	Ref.
He	SCC15, Oral	15 min	50	57%	22
He	SCC-QLL1, Oral	15 min	50	63%	22
He	SCaBer, Bladder	4 min	140	30%	23
He	SCaBer, Bladder	4 min	295	1.6%	23
Ar	U251SP, Glioblastoma	2 min	34	12%	24
He	HCT116, Colon	2 min	832	55%	15
He	Lu1205, Melanoma	2 min	832	33%	15
Ar	NCI-N87, Gastric	10 min	4	79%	25
Ar	NCI-N87, Gastric	30 min	0.6	72%	25
Air	Hela, Cervical	5 min	32.3	30%	26
Ar	ES2, Ovarian	10 min	471	18%	27
Ar	SKOV3, Ovarian	10 min	471	6%	27
Ar	LN229, Glioblastoma	9 min	220	4%	28
Ar	LN229, Glioblastoma	5 min	125	4%	28
Ar	LN229, Glioblastoma	9 min	74	7%	28
Ar	LN229, Glioblastoma	9 min	80	8%	28
Ar	LN229, Glioblastoma	9 min	64	12%	28
Ar	LN229, Glioblastoma	7 min	42	37%	28
Ar	LN229, Glioblastoma	9 min	33	42%	28
Ar	LN229, Glioblastoma	5 min	37	52%	28
Ar	LN229, Glioblastoma	5 min	32	53%	28
Ar	LN229, Glioblastoma	5 min	20	73%	28
Ar	LN229, Glioblastoma	5 min	33	76%	28
He	MDA-MB-231, Breast	1 min	135	85%	29
He	MDA-MB-231, Breast	1 min	90	76%	29
He	MDA-MB-231, Breast	1 min	70	75%	29

He	MDA-MB-231, Breast	1 min	45	59%	29
He	MDA-MB-231, Breast	1 min	35	63%	29
He	MDA-MB-231, Breast	1 min	38	71%	29
He	MDA-MB-231, Breast	1 min	30	69%	29
He	MDA-MB-231, Breast	1 min	32	71%	29
He	MDA-MB-231, Breast	1 min	30	73%	29
He	PA-TU-8988T, Pancreas	1 min	135	75%	29
He	PA-TU-8988T, Pancreas	1 min	90	61%	29
He	PA-TU-8988T, Pancreas	1 min	70	64%	29
He	PA-TU-8988T, Pancreas	1 min	45	63%	29
He	PA-TU-8988T, Pancreas	1 min	35	68%	29
He	PA-TU-8988T, Pancreas	1 min	38	85%	29
He	PA-TU-8988T, Pancreas	1 min	30	86%	29
He	PA-TU-8988T, Pancreas	1 min	32	94%	29
He	PA-TU-8988T, Pancreas	1 min	30	96%	29
He	U87MG, Glioblastoma	120 s	7.8	60%	16
Ar	MiaPaca-2, Pancreatic	10 min	20	94%	30
Ar	MiaPaca-2, Pancreatic	10 min	47	84%	30
Ar	MiaPaca-2, Pancreatic	10 min	81	47%	30
Ar	MiaPaca-2, Pancreatic	10 min	188	24%	30
Ar	MiaPaca-2, Pancreatic	10 min	327	14%	30
Ar	BxPc3, Pancreatic	10 min	23	99%	30
Ar	BxPc3, Pancreatic	10 min	41	96%	30
Ar	BxPc3, Pancreatic	10 min	93	28%	30
Ar	BxPc3, Pancreatic	10 min	163	26%	30
Ar	BxPc3, Pancreatic	10 min	377	21%	30
He	MDAMB231, Breast	5 min	212	41%	31
He	MDAMB468, Breast	5 min	212	46%	31

He	SaOS-2, Osteosarcoma	1-15 min	241	5%	32
He	SaOS-2, Osteosarcoma	1-15 min	241	3%	32
He	SaOS-2, Osteosarcoma	1-15 min	575	3%	32
Ar	A549, Lung	3 min	115	5%	33
Ar	A549, Lung	3 min	105	9%	33
He	B16, Melanoma	15-60 s	17	92%	34
He	B16, Melanoma	15-60 s	44	75%	34
He	B16, Melanoma	15-60 s	14	71%	34
He	B16, Melanoma	15-60 s	61	63%	34
He	B16, Melanoma	15-60 s	30	48%	34
He	B16, Melanoma	15-60 s	43	39%	34
He	B16, Melanoma	15-60 s	70	23%	34
He	B16, Melanoma	15-60 s	71	16%	34
He	B16, Melanoma	15-60 s	90	8%	34
Ar	Ehrlich Ascites Carcinoma	60 min	46	63%	35
$He+O_2$	FaDu, Head and neck	12 min	1641	23%	36
$He+O_2$	FaDu, Head and neck	12 min	1641	40%	36
$He+O_2$	FaDu, Head and neck	12 min	171	51%	36
$He+O_2$	FaDu, Head and neck	12 min	178	54%	36
$He+O_2$	CAL27, Head and neck	12 min	1641	40%	36
$He+O_2$	CAL27, Head and neck	12 min	1641	55%	36
$He+O_2$	CAL27, Head and neck	12 min	171	63%	36
$He+O_2$	CAL27, Head and neck	12 min	178	68%	36
Air	T24, Bladder	20 min	11	55%	37
Air	J82, Bladder	20 min	11	61%	37
Air	NCI-H520, Lung	30 min	16	9%	38
Air	NCI-H520, Lung	30 min	3	20%	38
Ar	BxPC-3, Pancreatic	10 min	140	52%	39

Ar	PANC-1, Pancreatic	10 min	140	50%	39
Ar	BxPC-3, Pancreatic	10 min	280	14%	39
Ar	PANC-1, Pancreatic	10 min	280	16%	39
Ar	T98G, Glioblastoma	9 min	86	66%	40
Ar	U87, Glioblastoma	9 min	86	49%	40
Ar	LN18, Glioblastoma	9 min	86	42%	40
Ar	LN229, Glioblastoma	9 min	86	36%	40
Ar	U251, Glioblastoma	9 min	86	28%	40
Ar	T98G, Glioblastoma	9 min	22	85%	40
Ar	U87, Glioblastoma	9 min	22	77%	40
Ar	LN18, Glioblastoma	9 min	22	82%	40
Ar	LN229, Glioblastoma	9 min	22	85%	40
Ar	U251, Glioblastoma	9 min	22	77%	40

Table S4. Primary antibodies used in this study.

Antibody	Catalog Number	Isotype	Clones	Company	MW (kDa)	Working Dilutions
HK1	2024#	Rabbit IgG	Monoclonal	CST[a]	102	1:800
HK2	2867#	Rabbit	Monoclonal	CST	102	1:800
PKM1/2	3190#	Rabbit IgG	Monoclonal	CST	60	1:1000
PKM2	4053#	Rabbit IgG	Monoclonal	CST	60	1:1000
PDK1	3205#	Rabbit IgG	Monoclonal	CST	43	1:1000
LDHA	2012#	Rabbit	Polyclonal	CST	37	1:1000
HIF-1α	14179#	Rabbit	Monoclonal	CST	120	1:1000
pmTOR^{S2448}	5536#	Rabbit IgG	Monoclonal	CST	289	1:800
mTOR	2983#	Rabbit	Monoclonal	CST	289	1:1000
pAKT^{S473}	4060#	Rabbit IgG	Monoclonal	CST	60	1:800
pAKT^{T308}	13038#	Rabbit IgG	Monoclonal	CST	60	1:800
AKT	4691#	Rabbit IgG	Monoclonal	CST	60	1:1000
p-eIF2α	5324#	Rabbit IgG	Monoclonal	CST	38	1:1000
eIF2α	3398#	Rabbit IgG	Monoclonal	CST	38	1:1000
PERK	20582#	Rabbit	Polyclonal	Proteintech[b]	150	1:500
p-ERK1/2	4376#	Rabbit IgG	Monoclonal	CST	42/44	1:1000
ERK1/2	16443	Rabbit	Polyclonal	Proteintech	38-44	1:1000
KEAP-1	227828#	Rabbit IgG	Monoclonal	Abcam[c]	70	1:2000
NCOA4	A5695	Rabbit IgG	Monoclonal	ABclonal[d]	70	1:1000
β-Actin	926-42210#	Rabbit IgG	Monoclonal	LI-COR[e]	45	1:1000

[a]CST=Cell Signaling Technology, MA, USA; [b]Proteintech=Proteintech Group, Wuhan, China; [c]Abcam= Abcam, Cambridge, UK; [d]ABclonal=ABclonal Technology, Wuhan, China; [e]LI-COR= LI-COR Biosciences Company, NE, USA.

Table S5. Lactate production (ng/μL) before and after Tri-CAP treatment.

	0h		6h		48h	
Cell Type	Mean (*n*=4)	Standard deviation	Mean (*n*=4)	Standard deviation	Mean (*n*=4)	Standard deviation
Ba/F3 Parental	7.569	3.001	2.695	1.109	7.143	1.910
Ba/F3 BCR-ABL1^{P210}	10.447	0.232	5.949	1.936	6.214	0.854
Ba/F3 BCR-ABL1^{T315I}	16.557	0.378	4.235	0.411	6.110	0.560

Table S6. Details of $CD34^+$ primary cells from CML patients and healthy individuals.

Category	Tissues	Cell type	BCR-ABL1 Kinase Domain Mutation	Assay
C5	Blood	CD34+	BCR-ABL1 native	Trypan blue-stained, Clonogenic
C6	Blood	CD34+	BCR-ABL1 ^{T315I}	Trypan blue-stained, Annexin, Clonogenic
C7	Blood	CD34+	BCR-ABL1 ^{T315I}	Trypan blue-stained, Annexin, Clonogenic
C8	Blood	CD34+	BCR-ABL1 native	Trypan blue-stained, Clonogenic
N9	Cord blood (single donor)	CD34+	NONE, healthy individual	Trypan blue-stained, Annexin, Clonogenic
N10	Cord blood (multiple donors pooled)	CD34+	NONE, healthy individual	Trypan blue-stained, Annexin, Clonogenic

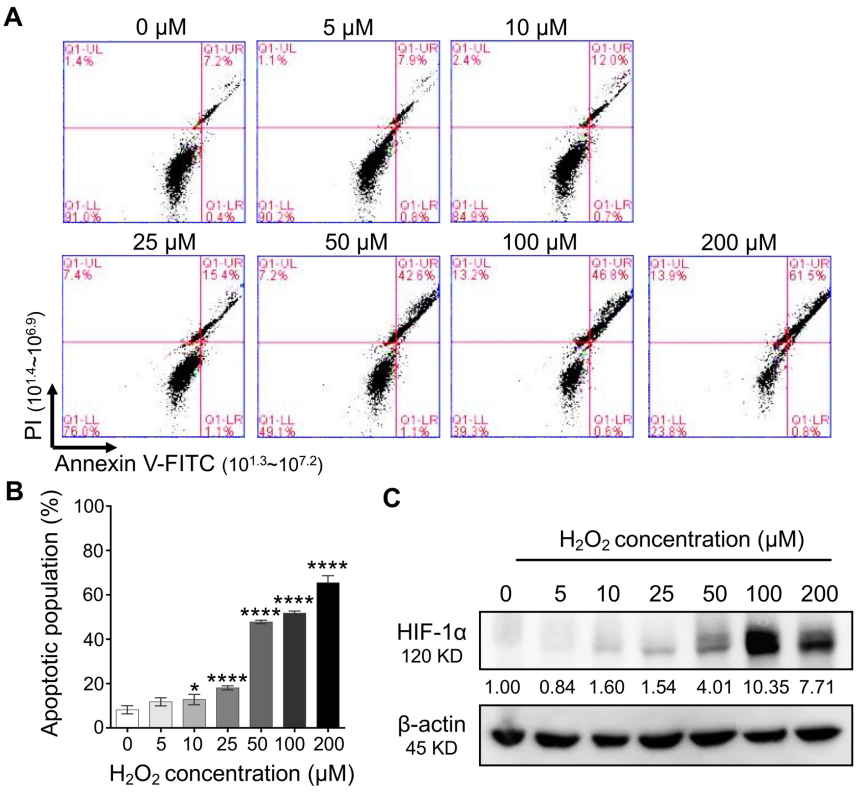

Fig. S1. **Apoptosis and HIF-1a protein expression after H_2O_2 treatment**. In resistant BCR-ABL1^{T315I} cells, (*A*) flow cytometry analysis of apoptotic cell populations; (*B*) the apoptosis rate (*p <0.05, ****p < 0.0001, n = 3); and (*C*) HIF-1α protein expression after 24-h incubation with H_2O_2 at different final concentrations.

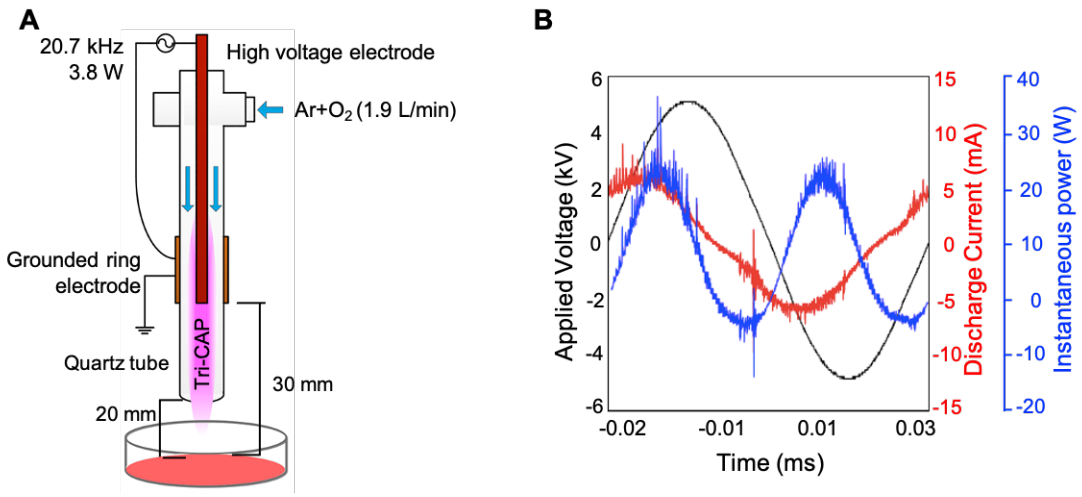

Fig. S2. **Basic characteristics the trident cold atmospheric plasma (Tri-CAP) system**. (*A*) Illustration of cell medium in a petri dish being treated with Tri-CAP in the form of a gas plasma jet in flowing argon mixed with 3% oxygen at 1.9 liter/min. The cell medium is 30 mm and 20 mm from the grounded electrode and the quartz tube, respectively. (*B*) Time traces of the applied voltage, discharge current, and instantaneous electrical power at an excitation frequency of 21.7 kHz and an average power of 3.8 W.

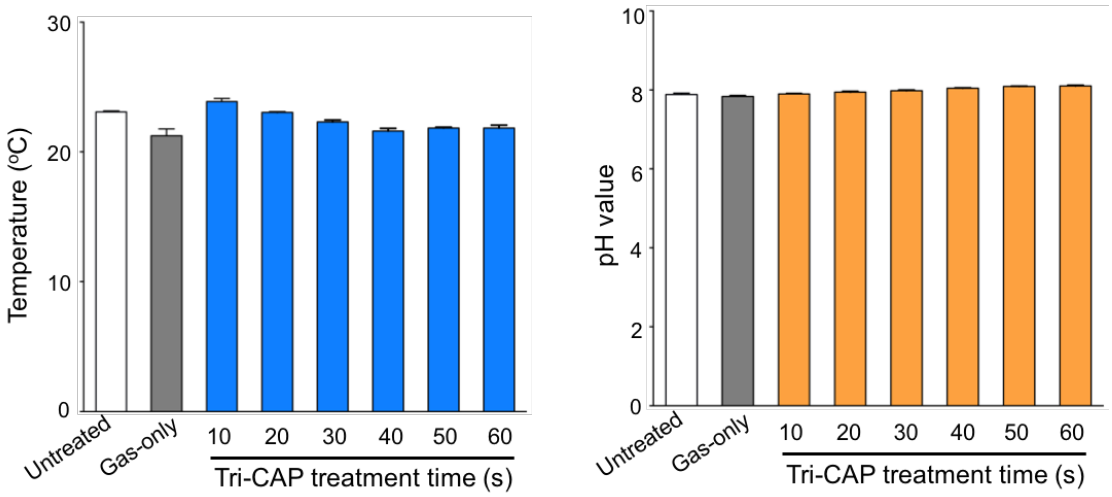

Fig. S3. Temperature and pH of cell-free RPMI-1640 medium as a function of Tri-CAP treatment time (n = 6). The starting temperature of the medium is 24°C.

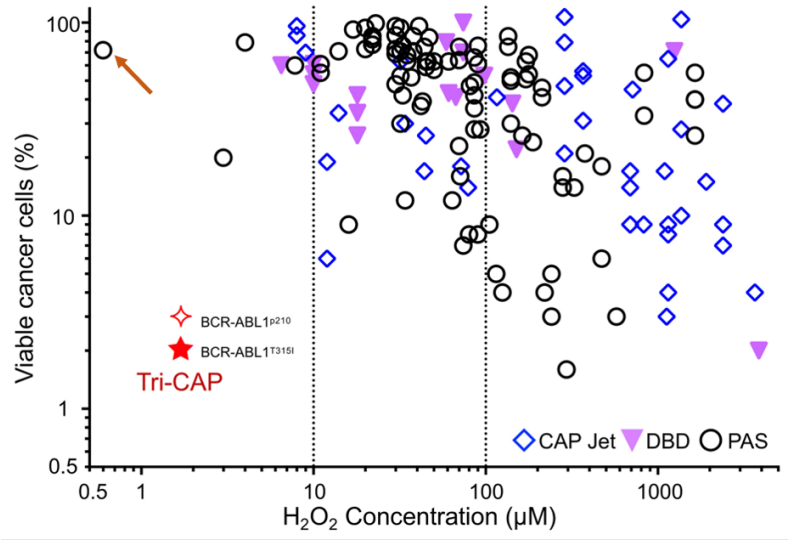

Fig. S4. **Tri-CAP explores a novel regime of H_2O_2 distinct to H_2O_2 levels associated with the vast majority of current CAP treatment regimens for cancer cells**. For a representative view of how Tri-CAP compares with literature data of CAP treatment of cancer cells, we present cell viability versus H_2O_2 for a total of 151 CAP treatment regimens for 53 cancer cell lines from reported studies of dielectric barrier discharge (DBD), CAP jets, and plasma-activated solution (PAS), listed in *SI Appendix* Table S1, S2 and S3, respectively. In 99% of all surveyed cases of current CAP treatment regimens (150/151), H_2O_2 levels used are markedly or significantly above 1.7 μM of H_2O_2 produced by Tri-CAP (Fig. 2*B* of the main text). The only exception (marked with an arrow) is associated with limited anticancer activity and high cancer cell viability of 72% (25), much above 2-3% in Tri-CAP-treated BCR-ABL1 cells (from Fig. 4*A* of the main text). Given these, we reason that Tri-CAP explores an uncharted regime of exceptionally low-level ROS for disrupting multiple cancer cell survival pathways and inducing robust cancer cell death.

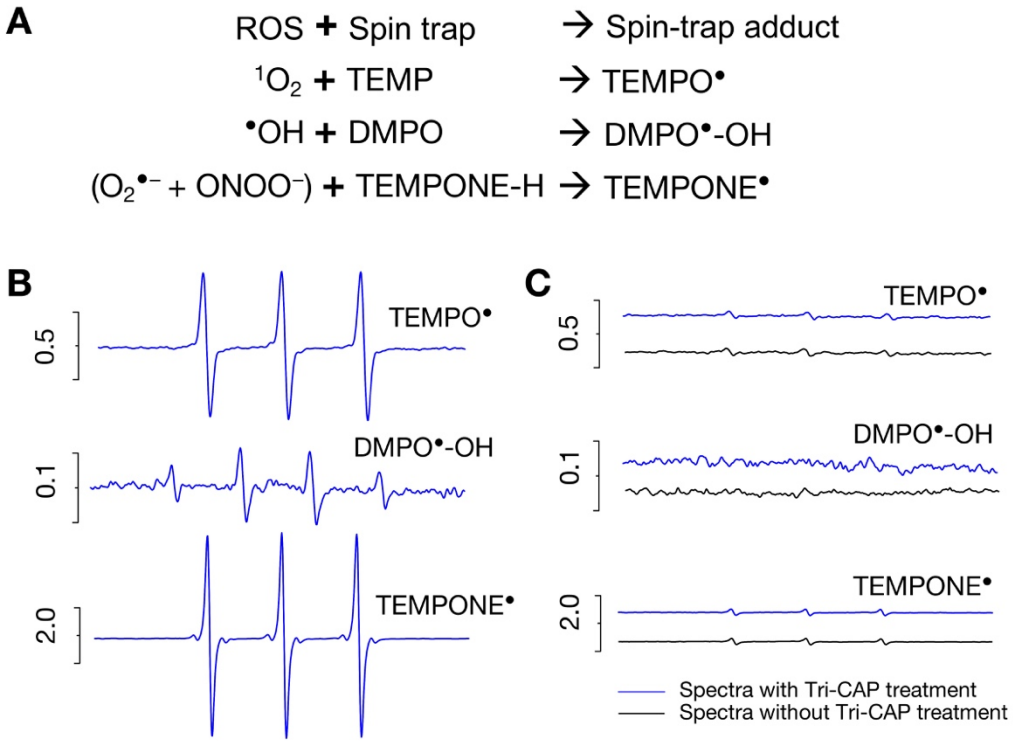

Fig. S5. **Measurement of short-lived reaction oxygen species (ROS) in cell-free medium using electron spin resonance (ESR) spectrometry and spin traps**. (*A*) Short-lived ROS in cell medium reacts with its spin trap to produce a spin-trap adduct; this is a free radical (shown with a superscript dot) whose concentration is deduced from its distinct ESR spectrum. The spin-trap adducts TEMPO•, DMPO•-OH, and TEMPONE• result from $^1O_2$, •OH, and the combination of $O_2^{\bullet-}$ and $ONOO^-$, respectively. (*B*) Distinct ESR spectra of TEMPO•, DMPO•-OH, and TEMPONE• following 60-s Tri-CAP treatment. (*C*) ESR spectra of TEMPO•, DMPO•-OH, and TEMPONE• ~30 s after Tri-CAP treatment and in untreated cell medium.

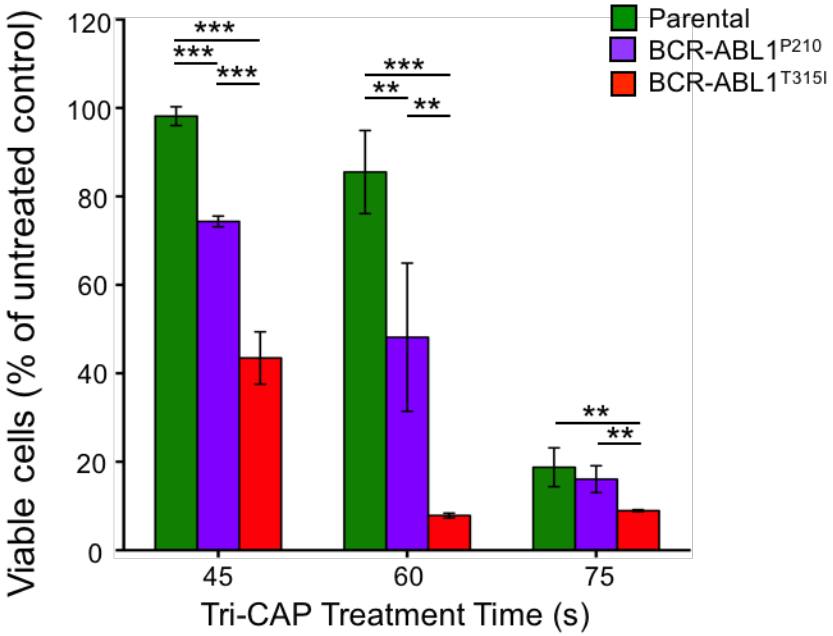

Fig S6. **Mouse Ba/F3 cell viability after Tri-CAP treatment**. Percent of viable imatinib-resistant BCR-ABL^{T315I}, imatinib-sensitive BCR-ABL^{p210}, and Ba/F3 parental cells at 72 h after Tri-CAP treatment for 45, 60, and 75 s. Cells are treated with Tri-CAP immediately after switching on the power supply; $n = 4$. $^{**}P < 0.01$; $^{***}P < 0.001$.

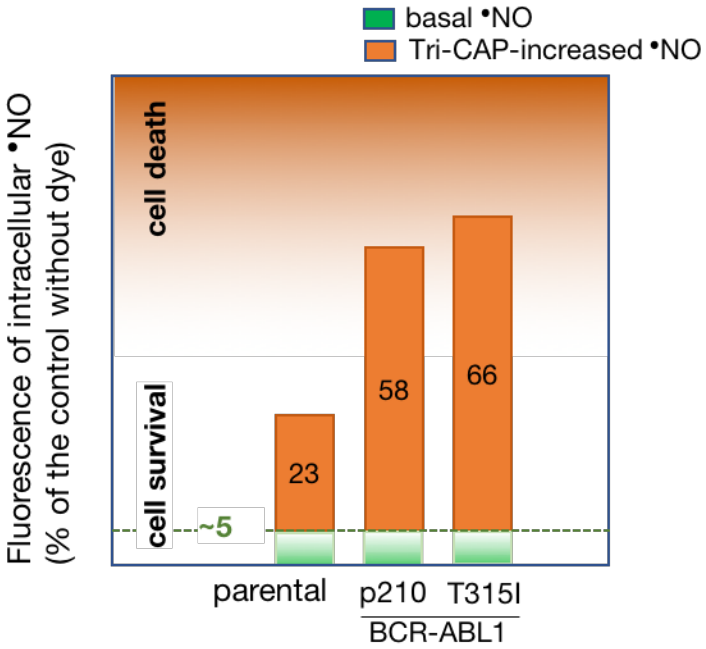

Fig. S7. Significant and preferential elevation of intracellular nitric oxide in BCR-ABL$^+$ cells in response to Tri-CAP treatment. Graph depicting the basal levels of intracellular $^{\bullet}$NO without Tri-CAP treatment and the peak level of intracellular $^{\bullet}$NO measured after 60-s Tri-CAP treatment.

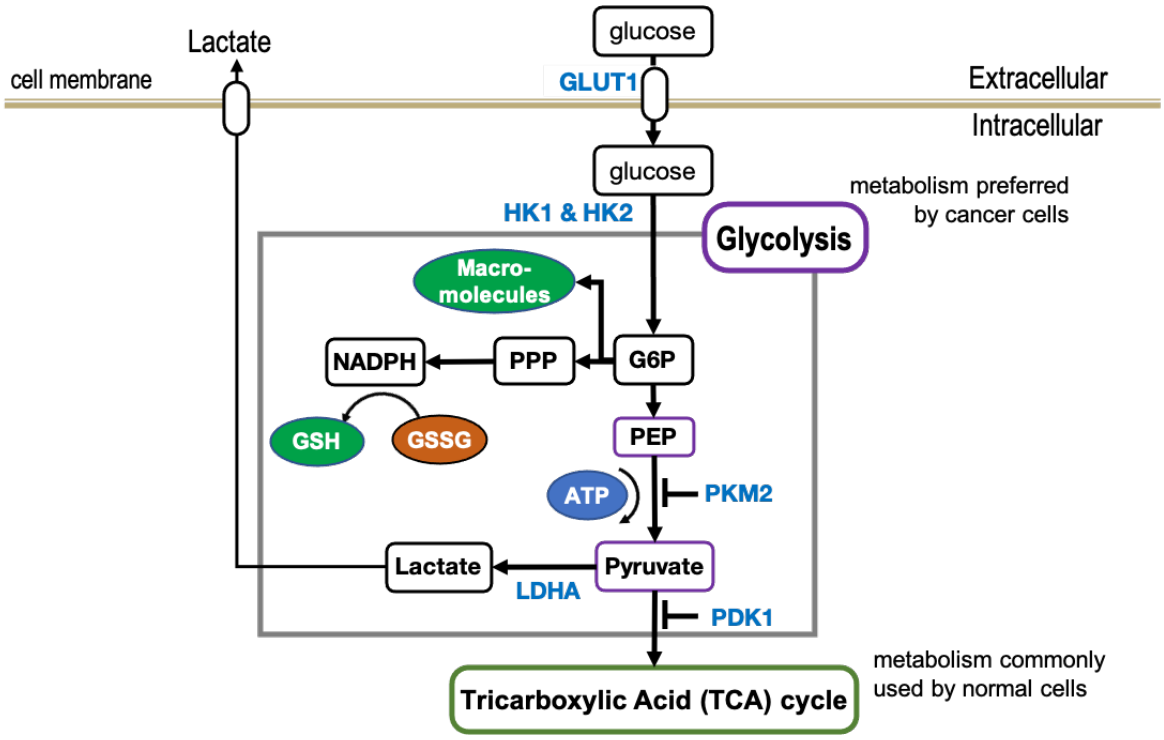

Fig. S8. **Schematic overview of strategy by which cancer cells use glycolysis for ATP production, macromolecule synthesis, and antioxidant regeneration.** Conversion of glucose to pyruvate mediated by glycolytic transporters (e.g., GLUT1) and enzymes facilitates production of ATP and lactate. This pathway is promoted by pyruvate dehydrogenase kinase 1 (PDK1), which limits glycolytic flux to tricarboxylic acid cycle (TCA) metabolism that is commonly used by non-malignant normal cells. Pyruvate kinase isozyme M2 (PKM2) decreases the rate of glucose-pyruvate conversion to promote glycolytic flux toward production of NADPH via the pentose phosphate pathway (PPP), as well as production of macromolecules. NADPH is reduced nicotinamide adenine dinucleotide phosphate and it replenishes GSH. Lactate promotes cancer cell growth. GLUT1, glucose transporter type 1; HK1 and HK2, hexokinase isoform 1/2; G6P, glucose 6-phosphate; PEP, phosphoenolpyruvic acid; LDHA, lactate dehydrogenase kinase A. Adapted from references (41, 42).

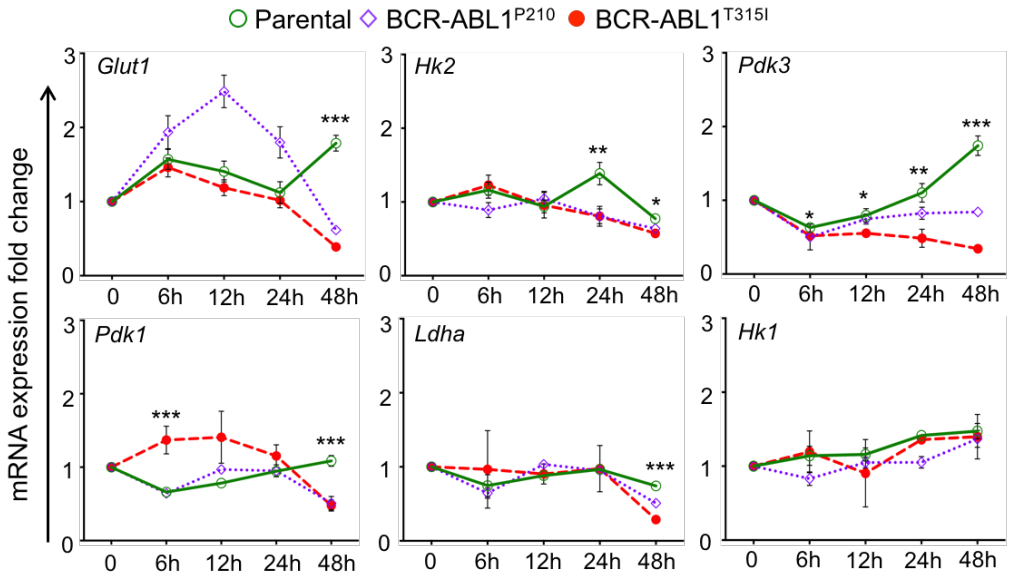

Fig. S9. Attenuated mRNA expression of glucose transporters and glycolytic enzymes in Tri-CAP-treated resistant BCR-ABL1^{T315I} cells. Time-course quantitative reverse transcriptase PCR (qRT-PCR) analysis of glycolysis-related gene expression in Tri-CAP-treated Ba/F3 parental, BCR-ABL1^{p210} and BCR-ABL1^{T315I} cells. *P*-values indicate statistical significance of the difference between BCR-ABL1^{T315I} and Ba/F3 parental cells (n = 3). **P* <0.05; ***P* <0.01; ****P* <0.001.

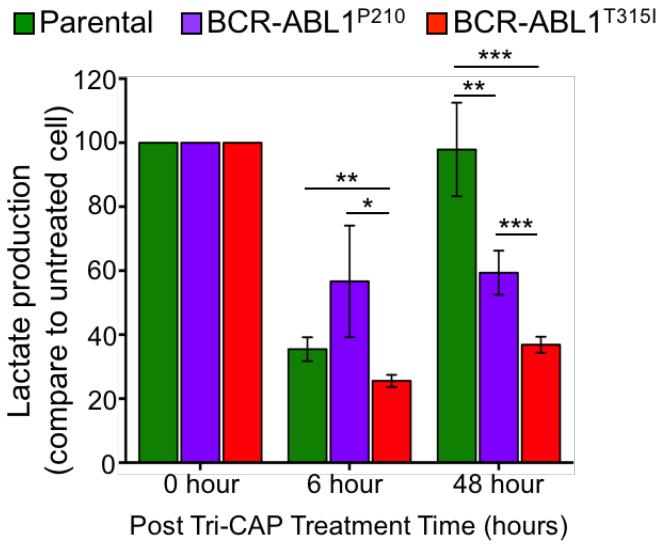

Fig. S10. Preferential reduction of lactate production in Tri-CAP-treated resistant BCR-ABL1^{T315I} cells. Normalized lactate production in Ba/F3 cell lines at 6 h and 48 h post-Tri-CAP treatment for 60 s (n = 4). At 48 h, BCR-ABL1^{T315I} cells display the largest reduction, and the parental cells recover to generate lactate levels that are similar to those produced before treatment. *P <0.05; **P <0.01; ***P <0.001.

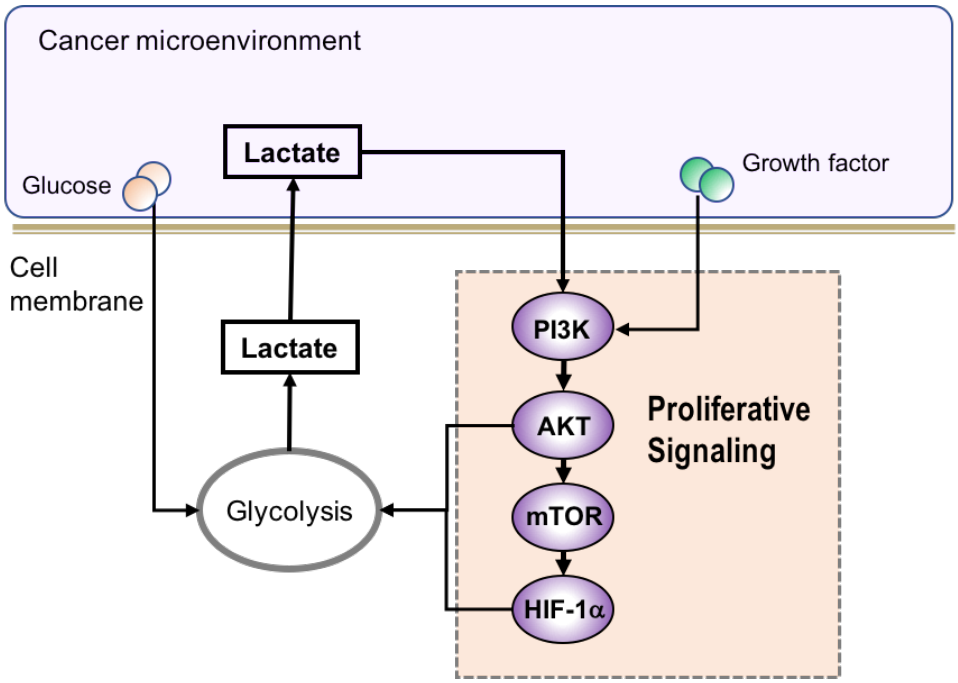

Fig. S11. **Glycolysis crosstalk with proliferative signaling perpetuates cancer survival.** Sustained proliferative signaling in dividing cancer cells via signaling molecules in the phosphoinositide 3-kinase (PI3K)/AKT/mammalian target of rapamycin (mTOR)/HIF-1α pathway (42). AKT and HIF-1α directly promote glycolytic metabolism, whereas lactate exported to the cancer microenvironment amplifies activity of PI3K/AKT signaling (43), thus perpetuating cancer survival.

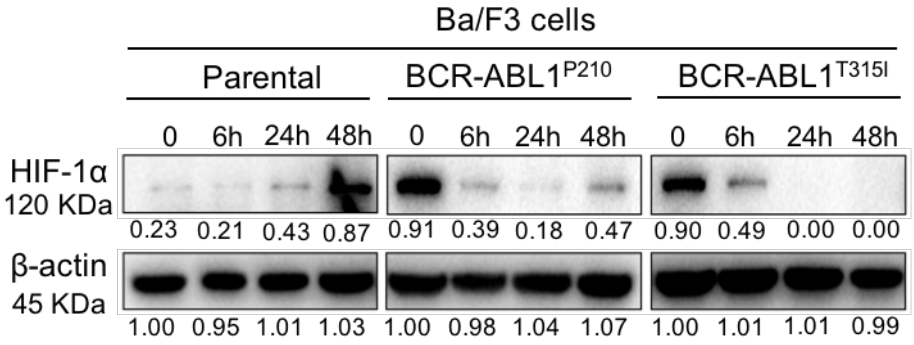

Fig. S12. Time-course of HIF-1α protein expression in Tri-CAP-treated Ba/F3 cells. Western blot analysis of HIF-1α at 6, 24, and 48 h post-Tri-CAP treatment for 60-s in Ba/F3 parental, BCR-ABL1^{P210}, and BCR-ABL^{T315I} cells; β-actin is used as a loading control. Antibodies are listed in Table S4.

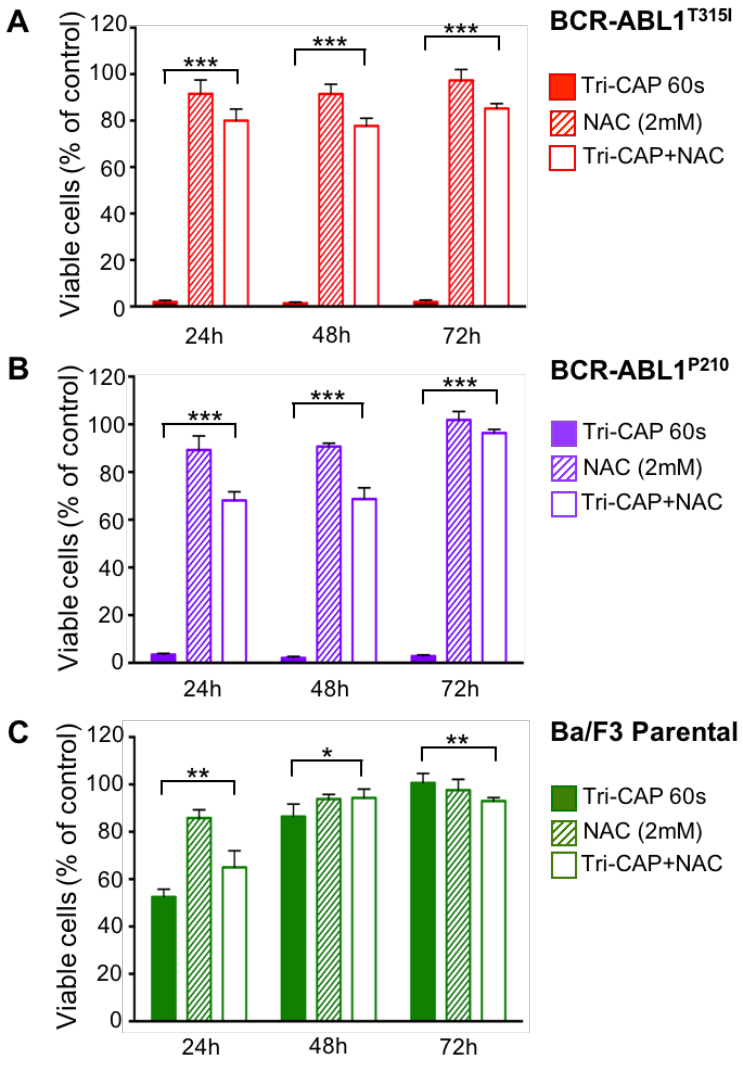

Fig. S13. ROS scavenger-mediated rescue of viability in Tri-CAP-treated BCR-ABL1^{+} cells. Viability of (*A*) BCR-ABL1^{T315I}, (*B*) BCR-ABL1^{p210}, and (*C*) Ba/F3 parental cells at 24, 48 and 72 h post-Tri-CAP treatment for 60-s with or without pretreatment with 2-mM N-acetyl-L-cysteine (NAC); $n = 6$. After Tri-CAP is switched on, it is left to run for 2 min before its treatment of cells. *P <0.05; **P <0.01; ***P <0.001.

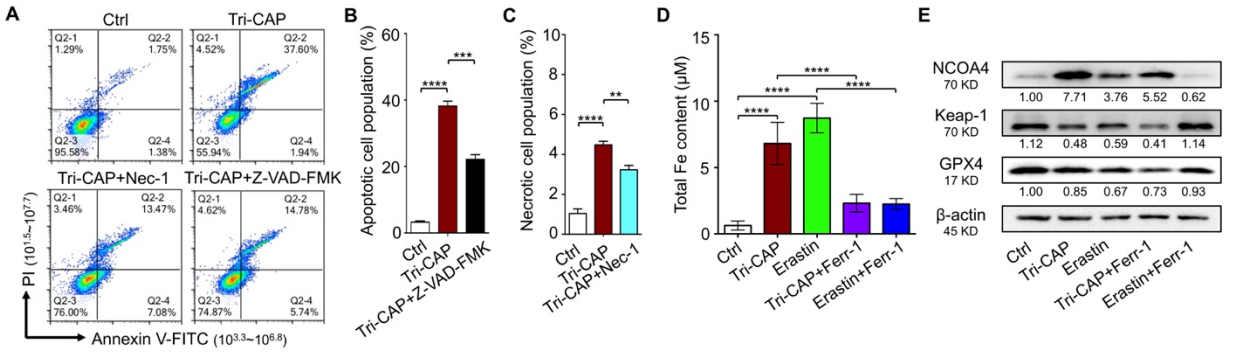

Fig. S14. **TRI-CAP induces diverse forms of cell death**. Pan-caspase inhibitor Z-VAD-FMK (20 μM), necrosis inhibitor necrostatin-1 (Nec-1) at 2 μM, and necroptosis inhibitor ferroptosis 1 (Ferr-1) at 1 μM are used to discriminate apoptosis, necrosis, and ferroptosis, whereas Erastin (2 μM) is used to induced ferroptosis. Their selected doses are commonly used in literature (44). To assess the presence of ferroptosis, we use three biomarkers, i.e., NCOA4 that promotes ferroptosis and Keap-1 and GPX4 that are negative regulators (45). In untreated (control) and Tri-CAP-treated BCR-ABL1^{T315I} cells, (*A*) apoptosis and necroptosis analysis using the Annexin V/Propidium iodide assay; (*B*) apoptotic and (*C*) necrotic population (n = 3, $^{**}P < 0.01$, $^{***}P < 0.001$, $^{****}P < 0.0001$); (*D*) cellular iron content at 24 h after Tri-CAP or Erastin treatment alone or with Ferr-1 (n= 3, $^{****}P < 0.0001$); (*E*) Western blot analysis of NCOA4, Keap-1 and GPX4 in the absence or presence of Ferr-1.

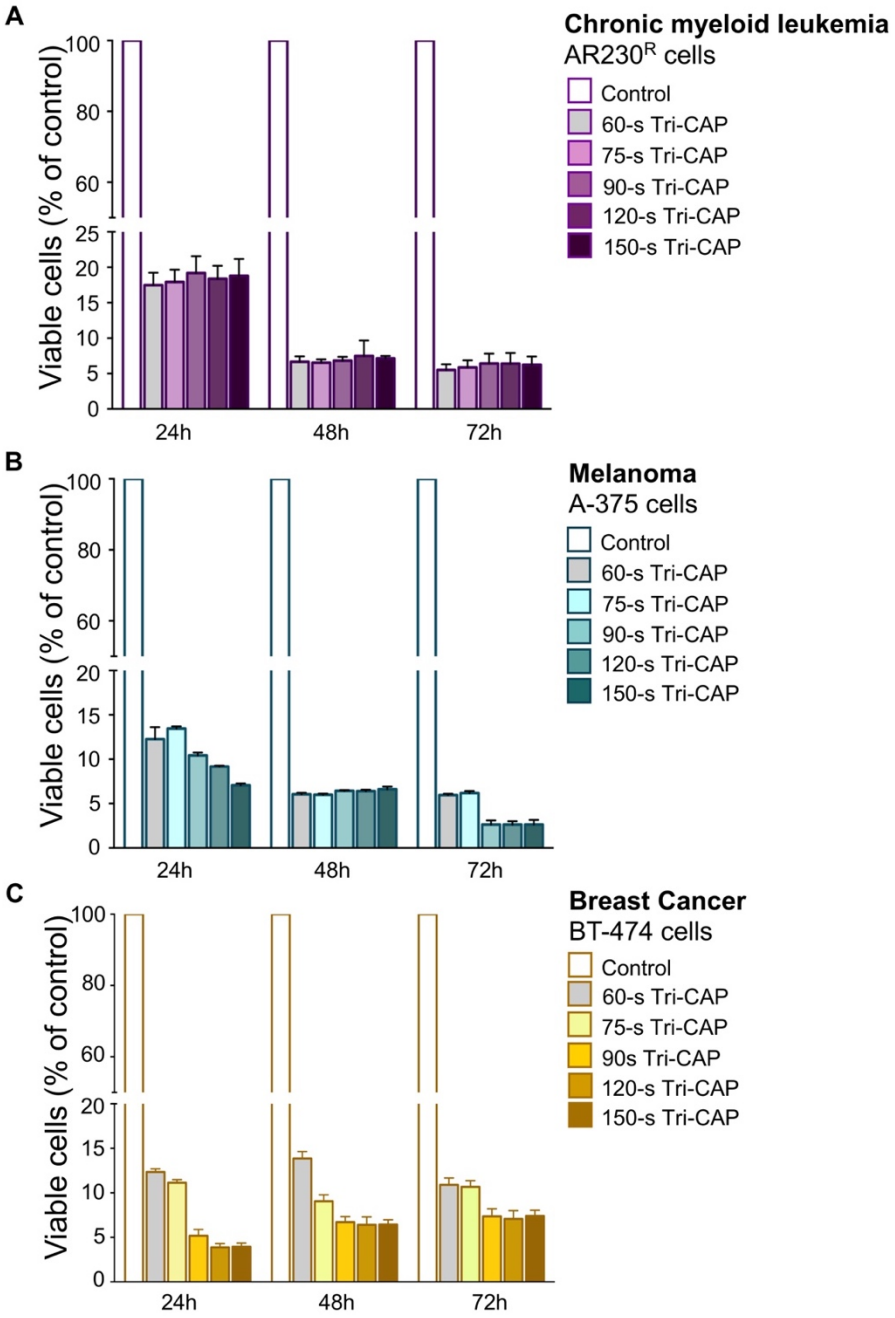

Fig. S15: **Viability of Tri-CAP-treated therapy-resisted human neoplastic cells**: Relative viability of (*A*) AR230R human CML cells, (*B*) A-375 human melanoma cells, and (*C*) BT-474 human breast cancer cells at 24, 48, and 72 h post-Tri-CAP treatment for 60–150 s; $n = 3$.

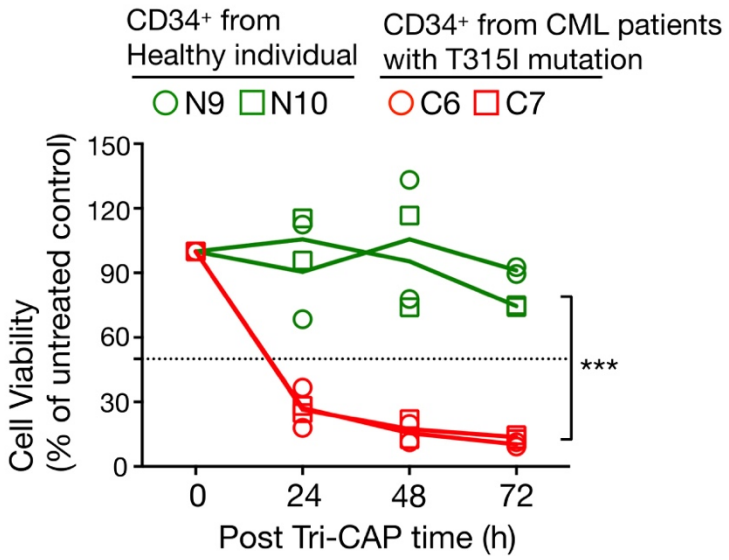

Fig. S16. Selective reduction in viability of CD34$^+$ haemopoietic stem and progenitor cells from CML patients in response to Tri-CAP treatment. Viability of CD34$^+$ cells from healthy individuals (green circles from N9 and squares from N10) and CD34$^+$ cells from CML patients harboring the T315I mutation (red circles from C6 and red squares from C7) at 24, 48, and 72 h post-Tri-CAP treatment for 60 s; two replicates each from two CML (C6 and C7) and two control (N9 and N10) cell populations. Primary CD34$^+$ cells from CML patients and healthy individuals are described in Table S6.

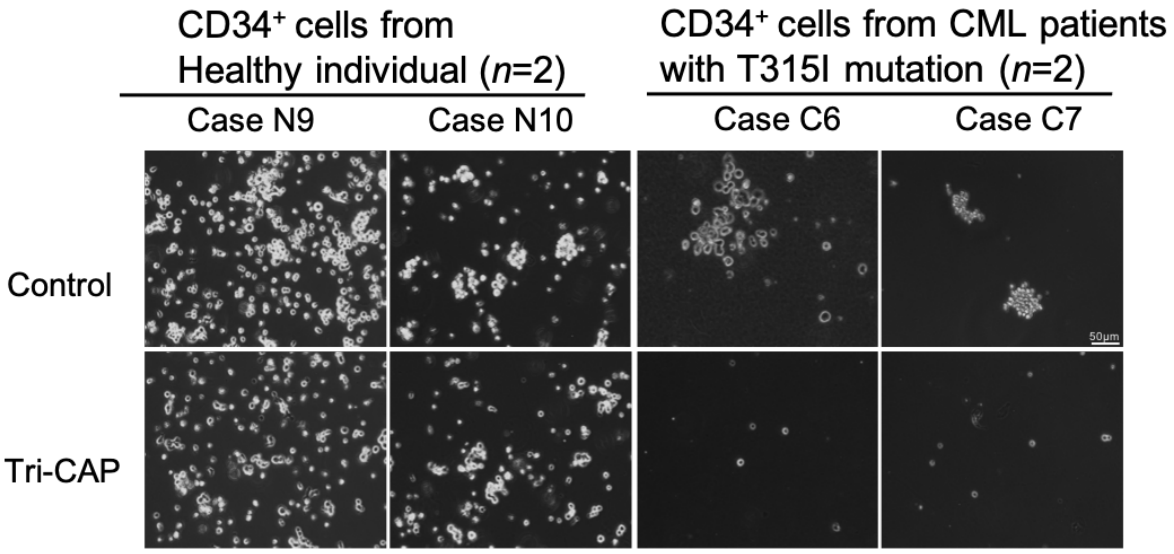

Fig. S17: **Microscope images of colonies formed by untreated and Tri-CAP-treated primary CD34$^+$ haemopoietic stem and progenitor cells from CML patients with BCR-ABL1^{T315I} and healthy controls**. Left panel: CD34$^+$ primary cells from healthy individuals N9 and N10. Right panel: CD34$^+$ primary cells from CML patients with the T315I mutation (patient C6 and patient C7). Tri-CAP-treated cells are imaged on day 7–14 after 60-s Tri-CAP treatment. Microscope magnification set at 20× for all graphs, and size is indicated with a 50-µm scale bar in the top right image associated with the untreated sample from patient C7. Cells from CML patients and healthy individuals are described in Table S6.

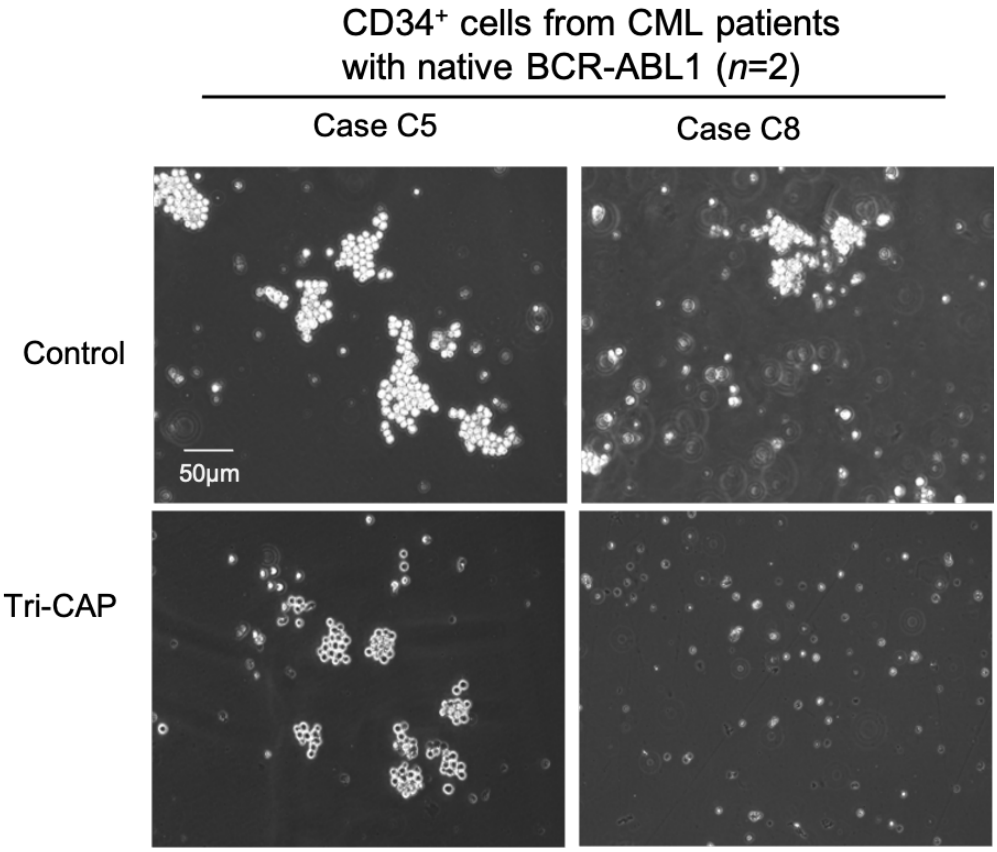

Fig. S18. **Microscope images of colonies of formed by untreated and Tri-CAP-treated primary CD34$^+$ haemopoietic stem and progenitor cells from CML patients with native BCR-ABL1**. CD34$^+$ primary cells from CML patients with native BCR-ABL1 of unknown mutation (patient C5 and patient C8). Tri-CAP-treated cells were imaged on day 7–14 after 60-s Tri-CAP treatment. Microscope magnification was set at 20× for all graphs, and size is indicated with a 50-µm scale bar in the top left image associated with patient C5. Cells from CML patients and healthy individuals are described in Table S6.

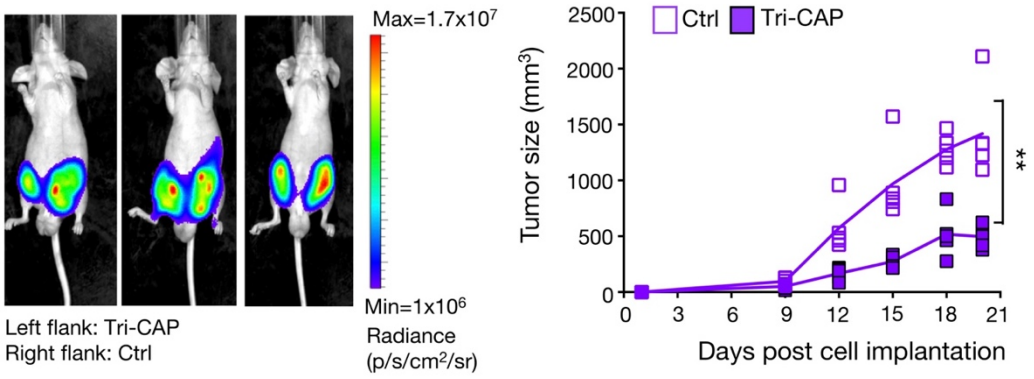

Fig. S19. Tri-CAP-treated BCR-ABL1^{p210} cells in mice show decreased tumor formation in mice. Tri-CAP-treated and untreated BCR-ABL1^{p210} cells are subcutaneously injected into the left and right flanks, respectively of each nude mouse. Left: bioluminescence images of mice on day 20 post-cell injection; Right: tumor size assessed once every three days; $n = 5$. ** $P < 0.01$.

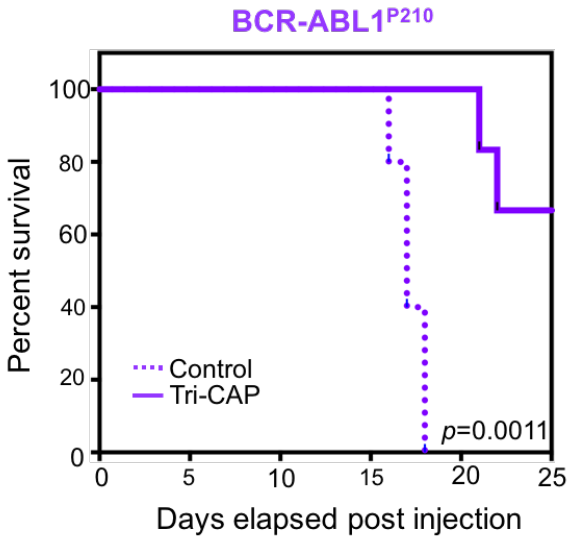

Fig. S20. Increased survival of mice harboring Tri-CAP-treated BCR-ABL1^{p210} cells. Survival curves of nude mice administered untreated or Tri-CAP-treated Ba/F3 BCR-ABL1^{p210} cells via tail vein injection; $n = 5$.

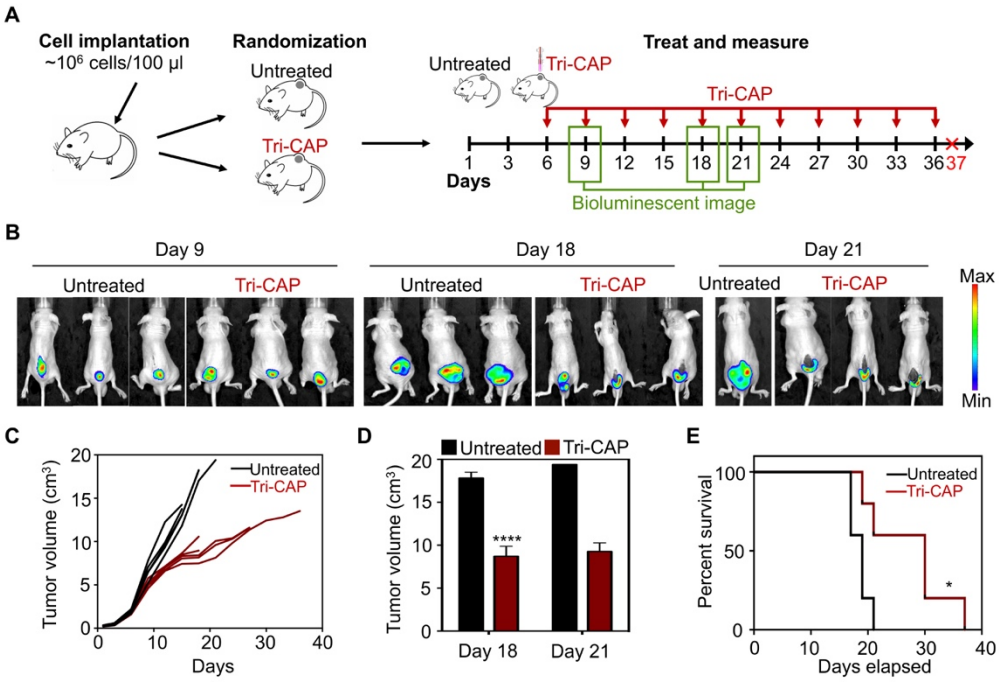

Fig. S21. Tri-CAP treatment of established tumor. (*A*) experiment design with nude mice treated once every 3 days from day 6 to 36; (*B*) tumor bioluminescence of untreated and Tri-CAP-treated mice ($n = 3$); (*C*) individual tumor kinetics; (*D*) tumor volume on day 18 ($n = 3$, ****$P < 0.0001$) and on day 21 when the control group is left with one mouse; (*E*) Kaplan-Meier survival kinetics for untreated and Tri-CAP treated mice ($n = 5$). *$P < 0.05$, log-rank test.

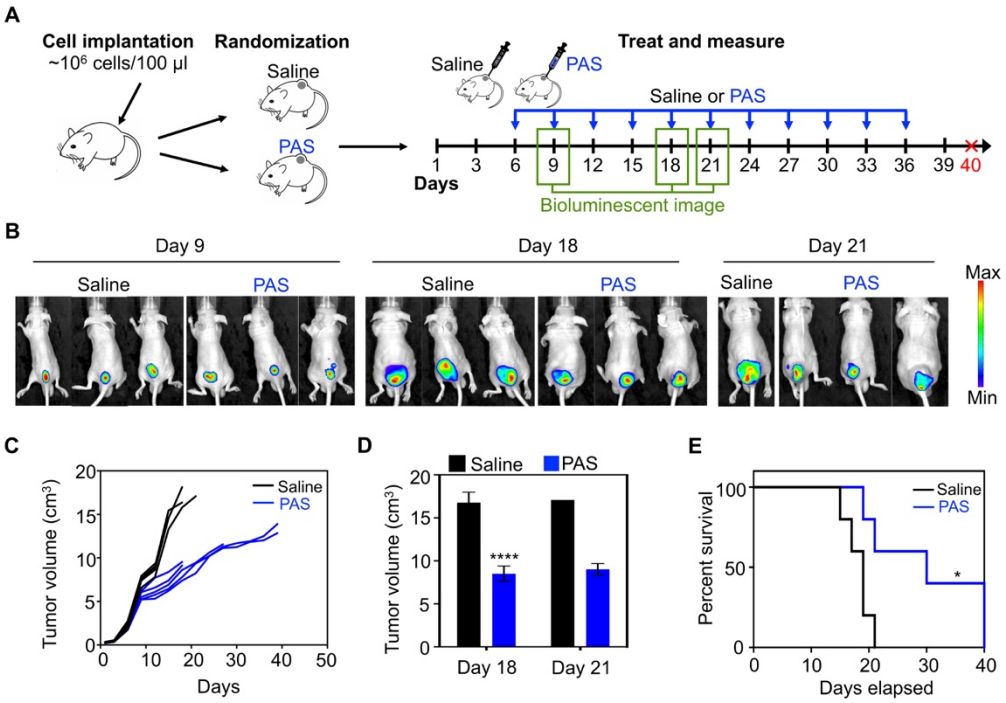

Fig. S22. Tri-CAP treatment of established tumor. (*A*) experiment design with mice treated once every 3 days from day 6 to 40; (*B*) tumor bioluminescence of untreated and PAS-treated mice ($n = 3$); (*C*) individual tumor kinetics; (*D*) tumor volume on day 18 ($n = 3$, $^{****}P < 0.0001$) and on day 21 when the control group is left with one mouse; (*E*) Kaplan-Meier survival kinetics for untreated and PAS-treated mice ($n = 5$). $^{*}P < 0.05$, log-rank test.

SI References

1. K. S. Louis, A. C. Siegel. Cell viability analysis using trypan blue: manual and automated methods. *Methods Mol. Biol*. **740,** 7–12 (2011).
2. T. O'Hare *et al*., AP24534, a Pan-BCR-ABL inhibitor for chronic myeloid leukemia, potently inhibits the T315I mutant and overcomes mutation-based resistance. *Cancer Cell* **16**, 401-412 (2009).
3. S. Bekeschus *et al*. A comparison of floating-electrode DBD and kINPen jet: plasma parameters to achieve similar growth reduction in colon cancer cells under standardized conditions. *Plasma Chem. Plasma Process* **38**, 1-12 (2018).
4. J. Koritzer *et al*. Restoration of sensitivity in chemo-resistant glioma cells by cold atmospheric plasma. *PLOS One* **8**, e64498 (2013).
5. V. Boxhammer et al. Bactericidal action of cold atmospheric plasma in solution. *New J. Phys*. **14**, 113042 (2012).
6. K. Panngom *et al*, Preferential killing of human lung cancer cell lines with mitochondrial dysfunction by nonthermal dielectric barrier discharge plasma. *Cell Death Disease* **4**, e642 (2013).
7. H. Yang *et al*. Effects pf atmospheric pressure cold atmospheric cold plasma on human hepatocarcinoma cell and its 5-fluorouracil resistant cell line. *Phys. Plasma* **22**, 122006 (2015).
8. J. Ma *et al*. Contribution of hydrogen peroxide to non-thermal atmospheric pressure plasma induced A549 lung cancer cell damage. *Plasma Process. Polym*. **14**, e1600162 (2017).
9. W. Nupangtha *et al*. A surface dielectric barrier discharge non-thermal plasma to induce cell death in colorectal cancer cells. *AIP Advances* **11**, 075222 (2021).
10. H. Mohamed *et al*. Differential effect of non-thermal plasma RONS on two human leukemic cell populations. *Cancers* **13**, 2437 (2021).
11. T. Sato, M. Yokoyama & K. Johkura. A key inactivation factor of HeLa cell viability by a plasma flow. *J. Phys. D: Appl. Phys*. **44**, 372001 (2011).
12. N. Kumar *et al*. Induced apoptosis in melanocytes cancer cell and oxidation in biomolecules through deuterium oxide generated from atmospheric pressure non-thermal plasma jet. *Sci. Rep*. **4**, 7589 (2014).
13. D. Xu *et al*. *In situ* OH generation from O_2^- and H_2O_2 plays a critical role in plasma-induced cell death. *PLoS One* **10**, e0128205 (2015).
14. N. Kumar, P. Attri, E. H. Choi & H. S. Uhm. Influence of water vapor with non-thermal plasma jet on the the apoptosis of SK-BR-3 breast cancer cells. *RSC Adv*. **5**, 14670 (2015).
15. P. M. Girard *et al*. Synergistic Effect of H_2O_2 and NO_2 in cell death induced by cold atmospheric He plasma. *Sci. Rep.* **6**, 29098 (2016).
16. Z. Chen *et al*. A novel micro cold atmospheric plasma device for glioblastoma both in vitro and in vivo. *Cancers*, **2017**, 9, 61 (2017).
17. G.-X. Xu, J.-R. Liu, Y.-M. Wu, X.-M. Shi & G.-J. Zhang. Low-temperature atmospheric pressure helium plasma jet damages malignant melanoma cells by inducing oxidative stress. *IEEE Trans. Plasma Sci*. 46, 2805-2813 (2018).
18. E. Gjika *et al*. Adaptation of operational parameters of cold atmospheric plasma for in vitro treatment of cancer cells. *ACS Appl. Mat. Interfaces* **10**, 9269-9279 (2018).
19. G. Chen *et al*. Transdermal cold atmospheric plasma-mediated immune checkpoint blockade therapy. *Proc. Natl. Acad. Sci. USA* **117**, 3687-3692 (2020).

20. G. Chen *et al*. Portable air-fed cold atmospheric plasma device for postsurgical cancer treatment. *Sci. Adv*. **7**, eabg5686 (2021).
21. C. Almeida-Ferreira *et al*. Open-air cold plasma device leads to selective tumor cell cytotoxicity. *Appl. Sci*. **11**, 4171 (2021).
22. S.-Y. Kim et al. Non-thermal plasma induces Akt degradation through turn-on the MUL1 E3 ligase in head and neck cancer. *Oncotarget* **6**, 33382-33396 (2015).
23. S. Mohades, N. Barekzi, H. Razavi, V. Marithamuthu & M. Laroussi. Temporal evaluation of the anti-tumor efficiency of plasma-activated media. *Plasma Process. Polym*. **13**, 1206-1213 (2016).
24. N. Kurake, *et al*. Cell survival of glioblastoma grown in medium containing hydrogen peroxide and/or nitrite, or in plasma-activated medium. *Arch. Biochem. Biophys.* **605,** 102-108 (2016).
25. Z. Chen *et al.* Treatment of gastric cancer cells with nonthermal atmospheric plasma generated in water. *Biointerphases* **11**, 0310101 (2016).
26. D. Boehm, C. Heslin, P. J. Cullen & P. Bourke. Cytotoxic and mutagenic potential of solutions exposed to cold atmospheric plasma. *Sci. Rep*. **6**, 21464 (2016).
27. K. Nakamura, *et al*. Novel intraperitoneal treatment with non-thermal plasma-activated medium inhibits metastatic potential of ovarian cancer cells. *Sci. Rep*. **7,** 6085 (2017).
28. W. van Boxem *et al*. Anti-cancer capacity of plasma-treated PBS: effect of chemical composition on cancer cell cytotoxicity. *Sci. Rep*. **7**, 16478 (2017).
29. D. Yan *et al*. The Strong Cell-based Hydrogen Peroxide Generation Triggered by Cold Atmospheric Plasma. *Sci. Rep.* **7**, 10831 (2017).
30. N. Kumar, P. Attri, S. Dewilde & A. Bogaerts. Inactivation of human pancreatic adenocarcinoma with atmospheric plasma-treated media and water: a comparative study. *J. Phys. D: App. Phys*. **51**, 255401 (2018).
31. L. Xiang, *et al*. Cold atmospheric plasma conveys selectivity on triple negative breast cancer cells both in vitro and in vivo. *Free Rad. Biol. Med.* **124**, 205-213 (2018).
32. J. Tornin et al. Pyruvate plays a main role in the antitumoral selectivity of cold atmospheric plasma in osteosarcoma. *Sci. Rep*. **9**, 10681 (2019).
33. A. Jo, H. M. Joh. T. H. Chung & J. W. Chung. Anticancer effects of plasma-activated medium produced by a microwave-excited atmospheric pressure argon plasma jet. *Oxid. Med. Cell. Longev.* **2020**, 1-17 (2020).
34. G. M. Xu *et al*. Characteristics of plasma activated medium produced by atmospheric pressure helium plasma jet and its selective effect on malignant melanoma and normal fibroblast cells. *IEEE Trans. Plasma Sci*. **48**, 587-593 (2020).
35. W. A. S. Brito *et al*. The anticancer efficacy of plasma-oxidized saline (POS) in the Ehrlich ascites carcinoma model in vitro and in vivo. *Biomedicine* **9**, 932 (2021).
36. K. Sklias, J. S. Sousa & P.-M. Girard. Role of short- and long-lived reactive species on the selectivity and anti-cancer action of plasma treatment in vitro. *Cancers* **13**, 615 (2021).
37. H. Zhang *et al*. The antitumor effect of plasma-activated saline on muscle-invasive bladder cancer cells in vitro and in vivo demonstrate its potential as a potential therapeutic approach. *Cancers* **13**, 1042 (2021).
38. C.-H. Song *et al.* Cocktail of reactive species generated by cold atmospheric plasma: oral administration induces non-small cell lung cancer cell death. *J. Phys. D: Appl. Phys.,* **54**, 185202 (2021).
39. N. Kumar *et al*. Physical plasma-derived oxidants sensitize pancreatic cancer cells to ferroptotic cell death. *Free Rad. Biol. Med*. **166**, 187-200 (2021).

40. P. Shaw, N. Kumar, A. Privat-Maldonado, E. Smits & A. Bogaerts. Cold atmospheric plasma increases temozolomide sensitivity of three-dimensional glioblastoma spheroids via oxidative stress-mediated DNA damage. *Cancers* **13**, 1780 (2021).

41. M. G. Vander Heiden, L. C. Cantley, C. B. Thompson. Understanding the Warburg effect: the metabolic requirements of cell proliferation. *Science* **324**: 1029-1033 (2009).

42. R. A. Cairns, I. S. Harris, T. W. Mak. Regulation of cancer cell metabolism. *Nat. Rev. Cancer* **11**, 85-95 (2011).

43. K. Xu *et al*., Glycolysis fuels phosphoinositide 3-kinase signaling to boost T cell immunity. *Science* **371**, 405-410 (2021).

44. H. Lee et al. Energy-stress-mediated AMPK activation inhibits ferroptosis. *Nat. Cell Biol*. 22, 225-234 (2020).

45. H. Zheng et al. Nanoparticle-induced ferroptosis: detection methods, mechanisms and applications. *Nanoscale* **13**, 2266- 2285 (2021).